

Parameterizing the Fresh-Water Flux from Land Ice to Ocean with Interactive Icebergs in a Coupled Climate Model

T. Martin^{a,1,*}, A. Adcroft^a

^a*Princeton University, Atmospheric and Oceanic Sciences Program, 201 Forrestal Road, Princeton, NJ 08540, USA.*

Abstract

Icebergs are an important part of the fresh-water cycle and, until now, have not been explicitly represented in Intergovernmental Panel on Climate Change (IPCC) class coupled global circulation models (CGCMs) of the climate system. In this study we examine the impact of introducing interactive icebergs in a next-generation CGCM designed for 21st Century climate predictions. The frozen fresh-water discharge from land is used as calving to create icebergs in the coupled system which are then free to evolve and interact with the sea-ice and ocean components. Icebergs are fully prognostic, represented as point particles and evolve according to momentum and mass balance equations. About 100,000 individual particles are present at any time in the simulations but represent many more icebergs through a clustering approach. The various finite sizes of icebergs, which are prescribed by a statistical distribution at the calving points, lead to a finite life-time of icebergs ranging from weeks, for the smallest icebergs (60 m length), up to years for the largest (2.2 km length). The resulting melt water distribution seen by the ocean enhances deep-water formation, in particular on the continental shelves, relative to the model without icebergs.

Keywords: coupled climate model, fresh-water flux, calving, icebergs, deep-water formation, Southern Ocean, Antarctica, Greenland

*Corresponding author, e-mail ToMartin@ifm-geomar.de, phone +49 431 600 4016, fax +49 431 600 4052

¹now at IFM-GEOMAR, Leibniz Institute of Marine Sciences, Duesternbrooker Weg 20, 24105 Kiel, Germany

1. Introduction

Calving of icebergs at the edge of glaciers and ice shelves is thought to account for as much as 50% of the net fresh-water flux from land ice to the ocean in Greenland, and 60-80% in the Antarctic (Hooke, 2005; Schodlok et al., 2006). The other principle mechanisms are surface melt in Greenland and bottom melt at the interface between the ice shelf and ocean in the Antarctic. Total mass loss from Antarctica and Greenland is estimated at 3200 ± 400 Gt yr⁻¹ of which 2300 ± 300 Gt yr⁻¹ is estimated to be due to calving alone (cf. Hooke, 2005, his Table 3.2). Although there is great uncertainty in these estimates, due to the challenge of making such observations, there is no doubt that calving and icebergs represent a significant pathway in the fresh-water cycle of the polar oceans.

In recent years, coupled global circulation models (CGCMs) of the climate system have striven to close the mass and energy budgets as well as possible. Only very few contemporary comprehensive CGCMs do already include an explicit model of ice sheets or ice shelves or a representation of interactive icebergs, but none actually include both. Precipitation over glaciated regions is often treated as excess fresh water (which would actually accumulate into an ice sheet in the real world) and is arbitrarily transported to the ocean. The choice of what to do with this excess fresh water is also arbitrary and greatly varies between models. An early and still often applied approach to close the fresh-water cycle is to redistribute this fresh-water excess uniformly and instantaneously across the global ocean (e.g. Boville and Gent, 1998). In a more advanced, but rarely used approach in the Hadley Center's Climate Model version 3 (HadCM3) the recirculation of excess precipitation is restricted to high latitude oceans, i.e. north of 40°N and south of 50°S (Weber et al., 2007). Although locally uniform in space this redistribution scheme also accounts for regional differences in the fresh-water flux from nearby ice sheets and is based on an estimated mean distribution of icebergs (Gordon et al., 2000).

In contrast, modern CGCMs have river networks, which are implemented in the land model, to transport the excess fresh water and bridge the gap. For example, in one approach all solid (or frozen) and liquid precipitation, which exceeds a buffer of 1000–2000 kg m⁻² snow water equivalent (or 1–2 m snow thickness) (Oleson et al., 2004; Weber et al., 2007), is exported in one

36 or more separate variables to the ocean using a river transport model. The
37 runoff is deposited in the coastal ocean at the river mouths. This solution is
38 widely used, for instance in the Community Climate System Model version 3
39 (CCSM3) (Oleson et al., 2004; Hack et al., 2006), the Climate Model version 2
40 (CM2.x) of the Geophysical Fluid Dynamics Laboratory (GFDL) (Anderson
41 et al., 2004), and many others (Weber et al., 2007).

42 Both approaches used in current CGCMs can be justified: Since little is
43 known about the amount and distribution of the solid fresh-water flux from
44 land to ocean (or calving flux) the river runoff scheme does not prescribe
45 any unknown quantity but simply closes the fresh-water cycle. However, this
46 approach implicitly assumes that the implied ice sheet is in instantaneous
47 equilibrium. In contrast, the approach taken by Gordon et al. (2000) helps to
48 minimize the bias of incorrect cold-fresh forcing by spreading out the forcing
49 while keeping it spatially restrained to ocean areas that are naturally affected
50 by a calving flux. Regardless of the choice of frozen discharge distribution,
51 no comprehensive coupled model has an explicit representation of interactive
52 icebergs.

53 In the real world, the calved mass takes the form of icebergs and ul-
54 timately enters the ocean in liquid form via the process of iceberg erosion
55 and melt. The two choices for calving distribution described above represent
56 two possible extremes for distributing the cold-fresh water forcing across the
57 ocean. In either case, forcing biases on the ocean should be expected, due to
58 the missing representation of icebergs; in the first instance, spreading out the
59 calving uniformly on the world oceans, the extra-polar regions should have a
60 false, albeit weak, fresh bias and a salty bias where icebergs are supposed to
61 melt. In the latter case of depositing calving into the coastal oceans, a fresh
62 bias might be expected at the coast and a salty bias where the missing ice-
63 bergs would otherwise melt. In practice, the story is more complicated than
64 this due to a tendency for the frozen discharge deposited into near-freezing
65 Antarctic coastal waters to immediately form sea ice which can then be ex-
66 ported away in frozen form. This might, at first glance, appear to be closer
67 to the way in which icebergs should export frozen water from the Antarctic
68 coast but the finite salinity of sea ice assumed by climate models, ironically,
69 leads to an export of salt relative to the icebergs which leads to a coastal
70 fresh bias.

71 The distribution of iceberg melt water was estimated by Bigg et al. (1997)
72 for the North Atlantic, and by Gladstone et al. (2001) and Silva et al. (2006)
73 for the Southern Ocean in uncoupled iceberg model experiments. They pre-

scribed a calving flux and simulated the drift and decay of icebergs forced by atmospheric reanalysis data and ocean model output. Recently, Jongma et al. (2009) examined the impact of distributed iceberg melt on the ocean by repeating the experiments of Bigg et al. (1997) and Gladstone et al. (2001) with a coupled atmosphere-sea-ice-ocean model of intermediate complexity ECBilt-CLIO (Opsteegh et al., 1998; Goose and Fichfet, 1999), which allowed the model ocean to actively respond to the prescribed calving and subsequent iceberg melt flux. Their findings can be summarized as follows: Iceberg mass and melt distributions exhibit a gradient perpendicular to the coast with the maximum at the coast. Icebergs generally follow the ocean surface circulation, for instance drifting with the Weddell Gyre or forming an "iceberg alley" past Newfoundland. In the uncoupled model experiments iceberg trajectories reach 50° N from the north, and 50° S from the south (though only 3% of the icebergs pass 63° S (Silva et al., 2006)), in the coupled runs they drift farther, reaching 40° N and 40° S in some places, respectively. The coupled experiments of Jongma et al. (2009) showed that the melt water from icebergs affects ocean salinity and temperature leading to an increase in Antarctic Bottom Water (AABW) formation of about 10% compared to a case with uniform calving flux redistribution. Finally, oceanic freshening and cooling due to iceberg melt increased the sea-ice area by 6–12% in these coupled experiments.

Uncoupled ice-ocean only models use salinity restoring to avoid climatic drift but introduce the added disadvantage of damping the response to fresh-water forcing. Modern coupled models do not have this problem (few CGCMs still rely on flux-correction or salinity-restoring). However, coupled models are inherently more non-linear and teasing out the response of the climate system to a particular forcing is inherently difficult in the presence of significant dynamic noise. For these reasons it is hard to anticipate whether the introduction of icebergs into a coupled model to better represent that part of the global fresh-water cycle will reproduce the significant response of an ice-ocean only model. The motivation for this study is thus three-fold: First, to better close the fresh-water cycle in a comprehensive climate model in preparation for introducing interactive ice-shelf models; second, to fix the known bias, due to depositing frozen discharge into the coastal ocean in the absence of icebergs; and third, to assess the impact on the ocean of introducing interactive icebergs into the coupled system.

In this study we apply the iceberg model of Bigg et al. (1997) and Gladstone et al. (2001) to a new comprehensive CGCM, which was created at the

112 GFDL. This coupled model system does not have an ice-sheet model but, as
 113 mentioned above, conveys excess snow to the coast. We will compare model
 114 results with and without the iceberg component. We will also compare our
 115 results with those of Jongma et al. (2009), who ran experiments with es-
 116 sentially the same iceberg model and with either the uniform redistribution
 117 approach applied only to the Southern Ocean south of 55°S or no calving
 118 flux at all for control experiments. The study presented here is the first
 119 that involves a full coupling of an iceberg model to a CGCM. In the absence
 120 of an explicit ice-shelf model, and hence without ice-shelf cavities, we feed
 121 the entire frozen fresh-water runoff into the iceberg model. In our coupled
 122 model the global calving rate amounts to 2200 Gt yr^{-1} on average, which
 123 compares well to the observational estimate of about 2300 Gt yr^{-1} (Hooke,
 124 2005) justifying our approach. Like Jongma et al. (2009) our presentation of
 125 results focusses on the Southern Ocean for three reasons: First, about 90%
 126 of the global iceberg mass is located there; second, the impact of the newly
 127 included iceberg component is strongest in this region; and third, to improve
 128 comparability to previous studies.

129 We begin our study by introducing the model components, in particular
 130 highlighting changes we made to the iceberg model in order to improve the
 131 numerical stability and impact of the icebergs. In Section 3 we present the
 132 results of our model experiments, followed by the comparison to observational
 133 data and results of other model studies in Section 4. In the latter section, we
 134 also discuss shortcomings of the present model before concluding our study
 135 in Section 5.

136 **2. The model**

137 *2.1. The coupled global circulation model*

138 Our numerical experiments are conducted with the coupled global circula-
 139 tion model CM2G, which was developed at GFDL to be used as a contri-
 140 bution to the upcoming Intergovernmental Panel on Climate Change (IPCC)
 141 Fifth Assessment Report (AR5). This model includes components for atmo-
 142 sphere, land, ocean and sea-ice processes. The atmosphere and land models
 143 are AM2 and LM2, respectively, which have been used successfully in the
 144 CM2.0 and CM2.1 models (e.g. Delworth et al., 2006) and are presented in
 145 more detail in Anderson et al. (2004). Here, it is important to note that the
 146 local snow cover may not exceed 1 m in LM2. Any frozen precipitation in
 147 excess of this buffer is exported to the ocean with a river transport model.

148 This calving flux only accounts for frozen runoff, though snow may melt and
149 then contribute to the liquid runoff.

150 The main difference between the CM2.x models and CM2G is the ocean
151 component which replaces the Modular Ocean Model (MOM) with a new
152 code, internally referred to as Generalized Ocean Layer Dynamics (GOLD).
153 GOLD is a descendent of the Hallberg Isopycnal Model (HIM) by Hallberg
154 (1995), which fundamentally differs from most ocean models in its vertical
155 coordinate which are isopycnals in the interior. Some details of the new
156 model can be found in Hallberg and Gnanadesikan (2006). An important
157 detail for our study is that GOLD treats the fresh-water cycle directly, i.e. it
158 does not use virtual salt fluxes to simulate fresh-water exchange to other
159 model components.

160 The sea ice simulator (SIS) has multiple ice thickness categories and com-
161 prises the three-layer-thermodynamics of Winton (2000) including a prognos-
162 tic snow cover. Sea-ice dynamics are based on the viscous-plastic rheology
163 of Hibler (1979) and are solved with the elastic-viscous-plastic approach of
164 Hunke and Dukowicz (1997). The sea ice is assumed to have a constant
165 salinity of 5.

166 We run the model on a global grid with a horizontal resolution of about
167 $1^\circ \times 1^\circ$ for ocean and sea ice and $2^\circ \times 2.5^\circ$ for atmosphere and land. The
168 atmospheric grid has 24 vertical levels and the oceanic 63.

169 This model setup is used to run a control experiment for comparison,
170 which will be identified by CTRL in the following.

171 *2.2. The iceberg model*

172 The iceberg model is based on the works of Bigg et al. (1997) and Glad-
173 stone et al. (2001). Individual icebergs are simulated as Lagrangian particles
174 in the Eulerian framework of the CGCM. In contrast to previous studies our
175 iceberg model is fully embedded in the coupled system. We further devel-
176 oped the model, improving its robustness and added bergy bits in a separate
177 experiment in order to study the effect of an extended iceberg lifetime. For
178 computational convenience the iceberg model is part of the sea-ice module
179 SIS in CM2G. The full set of equations of the iceberg model is given in
180 Appendix A.

181 *2.2.1. Iceberg formation*

182 Icebergs are land ice, i.e. consist of accumulated snow, and originate from
183 ice shelves or glaciers. As the coupled model does not explicitly simulate ice

Table 1: Iceberg size categories with iceberg length and total thickness, mass levels, mass scaling factor and calving distribution. The mass scaling factor gives the number of icebergs represented by one Lagrangian parcel in the calculations of iceberg dynamics. The calving distribution divides the calving flux into the various iceberg size categories prescribing an iceberg size distribution at the calving site. Iceberg sizes and frequency distribution are as in Gladstone et al. (2001, their Table 2).

category	length [m]	thickness [m]	mass [kg]	mass scaling	calving distribution
1	60	40	$8.8 \cdot 10^7$	2000	0.24
2	100	67	$4.1 \cdot 10^8$	200	0.12
3	200	133	$3.3 \cdot 10^9$	50	0.15
4	350	175	$1.8 \cdot 10^{10}$	20	0.18
5	500	250	$3.8 \cdot 10^{10}$	10	0.12
6	700	250	$7.5 \cdot 10^{10}$	5	0.07
7	900	250	$1.2 \cdot 10^{11}$	2	0.03
8	1200	250	$2.2 \cdot 10^{11}$	1	0.03
9	1600	250	$3.9 \cdot 10^{11}$	1	0.03
10	2200	250	$7.4 \cdot 10^{11}$	1	0.02

184 sheets and ice shelves we use the snow discharge from land to generate ice-
 185 bergs. In LM2 snow that falls on land may accumulate to a maximum of one
 186 meter. Excessive snow mass is conveyed to the coast using a river network.
 187 In the control run the snow is simply deposited in the coastal ocean. With
 188 the introduction of the iceberg model we implemented a storage for frozen
 189 runoff in each coastal grid cell. The snow mass entering a coastal grid cell is
 190 split into ten iceberg size categories according to a statistical distribution (see
 191 Table 1), which follows the suggestion of Gladstone et al. (2001) and is based
 192 on ship observations. Whenever the critical mass of the individual category
 193 is exceeded, an iceberg is released. In order to reduce computational cost
 194 the smallest particles are clustered together, released in groups and modeled
 195 as a single entity (see Table 1 for mass scaling). Although the Lagrangian
 196 particles may represent several icebergs, the thermodynamics of each iceberg
 197 in such a parcel is treated according to its original size. We simulate only
 198 icebergs with length scales of up to 2.2 km because we can assume that such
 199 small icebergs calve regularly (Schodlok et al., 2006). The calving storage is
 200 initialized with a random distribution avoiding a long spin-up of the climate
 201 simulation. New icebergs have a width to length ratio of 1:1.5 as suggested
 202 by Bigg et al. (1997), which is supported by observations (e.g. Jacka and
 203 Giles, 2007, and citations therein).

204 *2.2.2. Iceberg drift and decay*

205 In the model, iceberg drift is driven by drag by the atmosphere, sea ice
 206 and ocean as well as a wave radiation force. The momentum balance also
 207 includes Coriolis and pressure gradient forces. Three melting mechanisms
 208 describing iceberg ablation at or below the water line have been identified
 209 by Gladstone et al. (2001) to be of importance for the iceberg mass balance.
 210 This is influenced by the study of Løset (1993), which states that processes
 211 at the ice-air interface contribute only marginally to total iceberg ablation.
 212 The three mechanisms considered to be of importance are all described by
 213 empirical relationships. First, turbulence created by the difference of oceanic
 214 and iceberg motion leads to basal iceberg melt. The associated mass flux
 215 is derived proportional to this difference in motion, and the temperature
 216 difference between water and ice, where the iceberg is assumed to have a
 217 constant effective temperature of $-4\text{ }^{\circ}\text{C}$ (Løset, 1993). Second, we account
 218 for the effect of the buoyant convection along the sidewalls of the iceberg
 219 caused by the mentioned temperature contrast between iceberg and ocean.
 220 This melt flux is assumed to be solely a function of ocean temperature. A

221 third relationship describes the impact of waves on the iceberg. In proportion
 222 to the sea state and the ocean surface temperature we estimate a melt and
 223 erosion rate that includes the excavating of the iceberg at the water line as
 224 well as the calving of overhanging slaps as a result of extensive excavation.
 225 Here, sea state is a direct fit to the Beaufort scale. Further details are given
 226 in Appendix A.

227 The simulated icebergs only interact directly with the ocean’s surface
 228 layer. This does not take into account that icebergs of several hundred meter
 229 thickness reach into sub-surface layers. This shortcoming of the model is
 230 due to the implementation of the iceberg model in SIS forming a separate
 231 component in the coupled model system. Besides several advantages this
 232 includes the disadvantage that SIS only exchanges 2-D fields with the other
 233 model components.

234 Total energy in the CGCM is conserved because the iceberg parameteri-
 235 zation is only used to spatially distribute the frozen fresh-water runoff from
 236 land. The iceberg ”melt” flux is still returned as snow to the ocean model
 237 component as in CTRL and thus takes energy from the ocean to really melt,
 238 which leads to a cooling effect similar to real iceberg melt. In AM2/LM2
 239 snow has a constant temperature of 0 °C .

240 2.2.3. *Bergy bits*

241 The relationships for iceberg melt are empirically derived and thus incor-
 242 porate various subscale processes. It will be shown in Section 3.2 that the
 243 meltwater flux due to wave erosion dominates the fresh-water flux from ice-
 244 bergs. As described above, the wave erosion function does not only account
 245 for melting of ice at the iceberg’s surface but also for a partial break-up of
 246 the iceberg. Thus, wave erosion actually leads to the formation of small child
 247 icebergs, so-called bergy bits. These bergy bits are blocks of still solid ice
 248 and not liquid fresh water. As the ratio of liquid to solid mass flux is unclear
 249 for the wave erosion function, we carried out two experiments, one in which
 250 all wave erosion flux becomes liquid instantly (experiment BERG) as in the
 251 original iceberg model, and one in which the entire wave erosion mass flux is
 252 used to form solid bergy bits (BITS). The bergy bits are assumed to travel
 253 with their parent iceberg and melt according to the remaining two melt func-
 254 tions for basal and side wall melt. The World Meteorological Organization
 255 (WMO) describes bergy bits as ”large pieces of floating glacier ice, generally
 256 showing less than 5 m above sea level but more than 1 m and normally about
 257 100-300 m² in area” (WMO, 1989). In our model bergy bits are initialized as

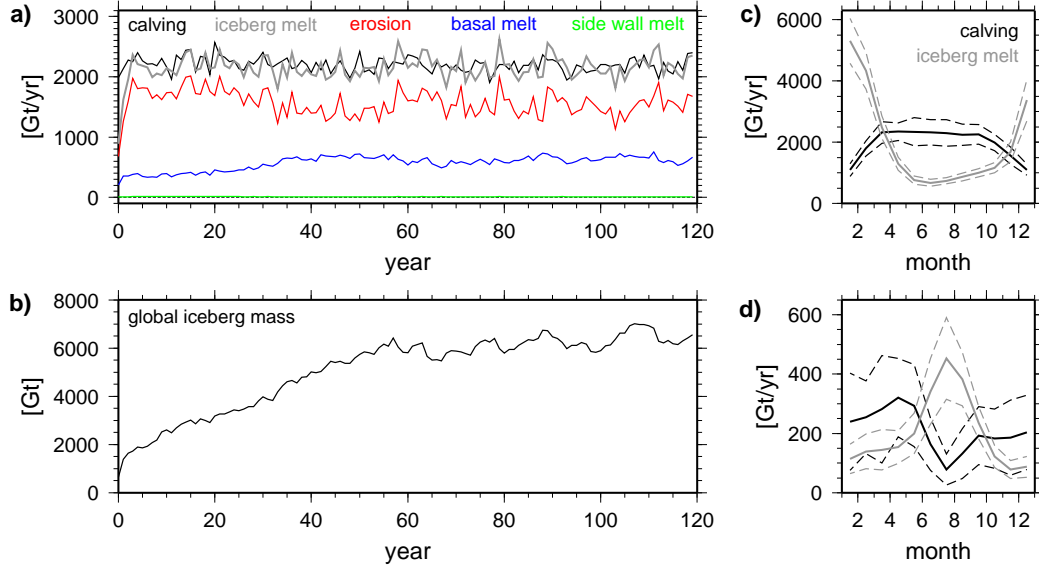


Figure 1: Results of experiment BERG. a) Time series of modeled calving flux (black) and iceberg melt rate (gray). The partitioning of the melt flux is depicted in red for wave erosion, blue for basal melt and green for side wall melt. b) Time series of global iceberg mass accumulated on the ocean. c) Mean annual cycle of calving (black) and iceberg melt (gray) for the southern hemisphere. d) same as panel c but for the northern hemisphere. Dashed lines mark plus/minus one standard deviation of the mean.

258 cubes with a side length of 40 m or less, not exceeding their parent iceberg's
 259 shortest dimension.

260 3. Results

261 3.1. Calving

262 The global calving flux available to iceberg formation in the CGCM
 263 amounts to a longterm, 100 year average of 2210 Gt yr^{-1} . This mass flux is
 264 robust across all our model experiments, varying only by 10 Gt yr^{-1} . The
 265 standard deviation, which indicates inter-annual variability, is 130 Gt yr^{-1}
 266 with a maximum difference of 10 Gt yr^{-1} between the experiments. Fig-
 267 ure 1a depicts the time series of experiment BERG (black line). The time
 268 series is dominated by inter-annual variations, multi-annual or decadal cycles
 269 are very weak. The global calving rate is dominated by the discharge from
 270 Antarctica, which amounts to $2000 \pm 130 \text{ Gt yr}^{-1}$ in our experiments. In the
 271 northern hemisphere, runoff from Greenland is largest with $210 \pm 40 \text{ Gt yr}^{-1}$

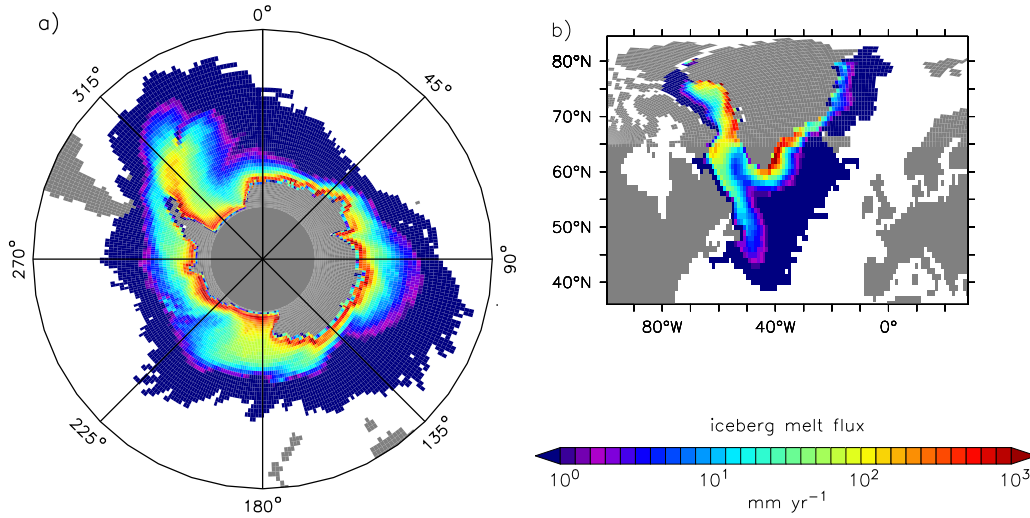


Figure 2: 100 year average of the fresh-water flux to the ocean in mm yr^{-1} from iceberg melt in experiment BERG for icebergs originating from a) Antarctica and b) Greenland. Note the use of a logarithmic color scale. The irregular outline is a consequence of the passage of individual large icebergs.

272 . Further, marginal contributions of less than 1 Gt yr^{-1} in total originate
 273 from, for instance, Alaskan and Himalayan glaciers.

274 On the southern hemisphere major snow discharge and therefore ice-
 275 berg calving sites in the model are located in the Ross ($150\text{--}200^\circ \text{W}$) and
 276 Amundsen seas ($95\text{--}120^\circ \text{W}$) as well as in the southwest of the Weddell Sea
 277 ($10\text{--}60^\circ \text{W}$). Discharge into the Davis Sea region ($80\text{--}110^\circ \text{E}$) is an order of
 278 magnitude smaller though still notable. About two thirds of all coastal grid
 279 cells around Antarctica have a calving flux of more than 1 Gt yr^{-1} .

280 In contrast, only one-third of the Greenlandic coastal grid cells have a
 281 significant calving flux. Important discharge sites are along the southeast
 282 coast and in the Disko Bay region ($\sim 70^\circ \text{N}$, 55°W).

283 Figures 1c and 1d depict the seasonal cycle of calving in the southern
 284 and northern hemispheres respectively. The frozen fresh-water discharge
 285 is directly linked to the precipitation having only a time lag of order 10
 286 days at maximum. The discharge rate from Antarctica is high during the
 287 winter months April to September when the snow cover of the continent is
 288 less exposed to solar radiation and warm temperatures causing surface melt.
 289 Though precipitation over Antarctica is greater during summer, the snow
 290 quickly melts and becomes liquid runoff during this season, and hence does

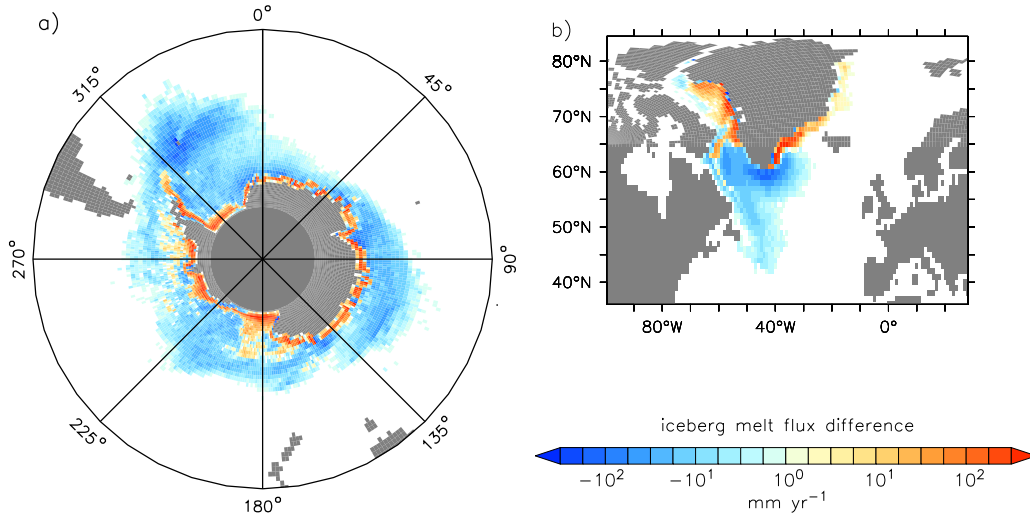


Figure 3: Difference BERG-BITS of the fresh-water flux due to iceberg melt in mm yr^{-1} for a) the Southern Ocean and b) the North Atlantic derived from 100 year averages of the two experiments. Blue colors indicate a greater iceberg melt water flux to the ocean in BITS than in BERG, red indicates a smaller flux in BITS.

not affect iceberg calving. In the northern hemisphere maximum calving occurs in April at the end of the winter season.

3.2. Icebergs

The iceberg mass accumulated on the ocean reaches its equilibrium after about 60 years (see Figure 1b), which means iceberg melt does not fully balance calving in the first 60 years of our experiments, though the meltwater flux reaches the same order of magnitude as calving already after 5 years (Figure 1a). In the equilibrium state roughly 100,000 individual icebergs are continuously present in the simulation. This number represents the dynamically active Lagrangian parcels and does not incorporate the mass scaling factor.

In Figure 1a the time series of the meltwater flux is presented together with its three components: the fluxes due to wave erosion, basal melt and side wall convection. With a global rate of 1550 Gt yr^{-1} (averaged over years 60–120) the wave erosion flux is clearly the largest contributor accounting for 70% of the total melt flux. It is 2.5 times greater than the basal melt flux on global average. The contribution by side wall melt does not exceed

308 17.5 Gt yr⁻¹ and is thus almost negligible. The wave erosion flux also has
309 the strongest inter-annual variations with amplitudes of up to 630 Gt yr⁻¹.

310 Iceberg melt has a maximum in January and July on the southern and
311 the northern hemisphere respectively (Figures 1c and 1d). In contrast to
312 the maximum of the calving flux the peak of iceberg melt is much more
313 pronounced because iceberg mass accumulates during winter and quickly
314 melts when the sea-ice cover retreats and ocean temperatures rise. Sea ice
315 plays an important role here as it insulates the ocean from the atmosphere
316 hindering radiative warming of the ocean surface and momentum exchange,
317 which both are important for the wave erosion to develop its full effect. In
318 the CTRL run, with the absence of icebergs, the two processes of calving
319 (i.e. snow discharge and fresh-water release to the ocean) appear as one,
320 which imposes a false timing for the melt of the frozen discharge. As shown
321 in Figure 1 calving and fresh-water release to the ocean have opposite annual
322 cycles. By introducing icebergs and a storage for the calving flux at the coast
323 these two processes are decoupled and have shifted the fresh-water release
324 correctly towards summer.

325 The spatial distribution of the meltwater flux depicted in Figure 2, which
326 shows results of BERG, is very similar to the mass distribution of icebergs
327 (not shown). The meltwater flux has a strong gradient perpendicular to the
328 coast, which is most prominent in the Southern Ocean. This agrees well
329 with the model results of Gladstone et al. (2001) and observational records
330 (Jacka and Giles, 2007). The maximum melt flux of up to 10³ mm yr⁻¹ is
331 located near the coast, where many of the small icebergs accumulate during
332 the winter and quickly decay in the subsequent summer season. For larger
333 icebergs two major export routes can be identified in the Southern Ocean.
334 The overall largest export is found in the western Weddell Sea where icebergs
335 follow the persistent gyre so that melt rates reach 10^{2.5} mm yr⁻¹ far off the
336 coast. The second largest export area is fed from the western Ross Sea region
337 and melt rates north of the Ross Sea exceed 10^{1.5} mm yr⁻¹. In these two
338 regions and additionally southwest of Australia icebergs penetrate far north.
339 Large icebergs can reach latitudes of 40° S in the Pacific sector and even 30° S
340 in the Atlantic and Indian Ocean sectors. East of Greenland icebergs follow
341 the East Greenland Current around the southern tip entering the Labrador
342 Sea from the east (Figure 2b). Icebergs coming from the Baffin Bay enter
343 the Labrador Sea from the north to form the famous iceberg alley passing
344 Newfoundland and penetrating into the North Atlantic as far south as 40° N
345 (Figure 2b).

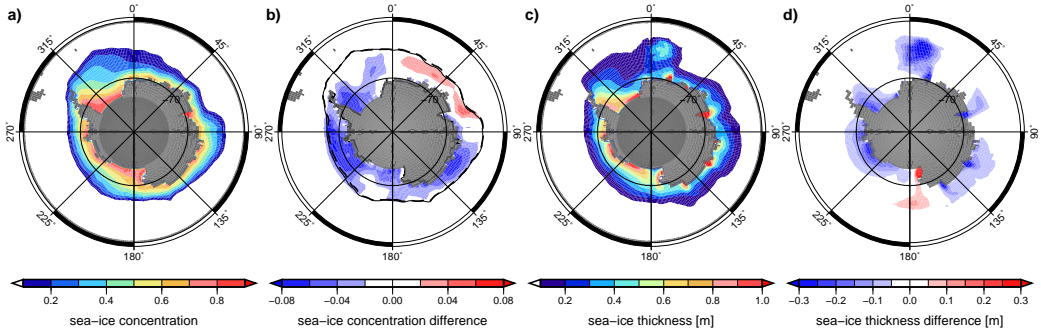


Figure 4: 100 year averages of sea-ice properties and their change due to the introduction of icebergs. a) Sea-ice concentration in CTRL. b) Concentration difference of BITS-CTRL. c) In-situ sea-ice thickness in m in CTRL. d) Thickness difference in m of BITS-CTRL.

Although the above major features of the spatial distribution of icebergs are very similar in both experiments, BERG and BITS, the introduction of the bergy bits reduces the fresh-water input close to the coast by up to $10^{2.5}$ mm yr⁻¹ (Figure 3), which is close to the magnitude of the total flux (Figure 2). The bergy bits delay the meltwater discharge to the ocean while they drift with their parent iceberg. This causes a wider distribution of the fresh-water input farther out at sea, where the flux in the BITS run exceeds those in the BERG experiment by up to 10^2 mm yr⁻¹ (Figure 3). This promotes the effect of the icebergs as will be shown in Section 3.4.

3.3. Sea ice

The introduction of icebergs lead to a reduction in sea-ice compactness and thickness in particular in the Southern Ocean. These changes are shown in Figure 4 as differences between the BITS and CTRL experiments along with the sea-ice concentration and thickness of the CTRL run. While the long-term mean position of the sea-ice edge in the Southern Ocean has only changed marginally, the fractional coverage is strongly reduced in about three-quarters of the sea ice covered area (Figure 4b). This means a loss of about 0.5×10^6 km² of sea-ice cover. The strongest decrease in sea-ice concentration of 6–8% is found in the Amundsen, Bellingshausen (70–95° W), Weddell, and D’Urville seas (110–150° E), i.e. along the major export routes of icebergs mentioned above. In these sectors the mean sea-ice extent has slightly decreased. In contrast, an increase in sea-ice concentration of up to 6% and a slightly greater extent is visible between 0° and 90° E. This increase in sea-ice area is associated with extensive iceberg melt occurring

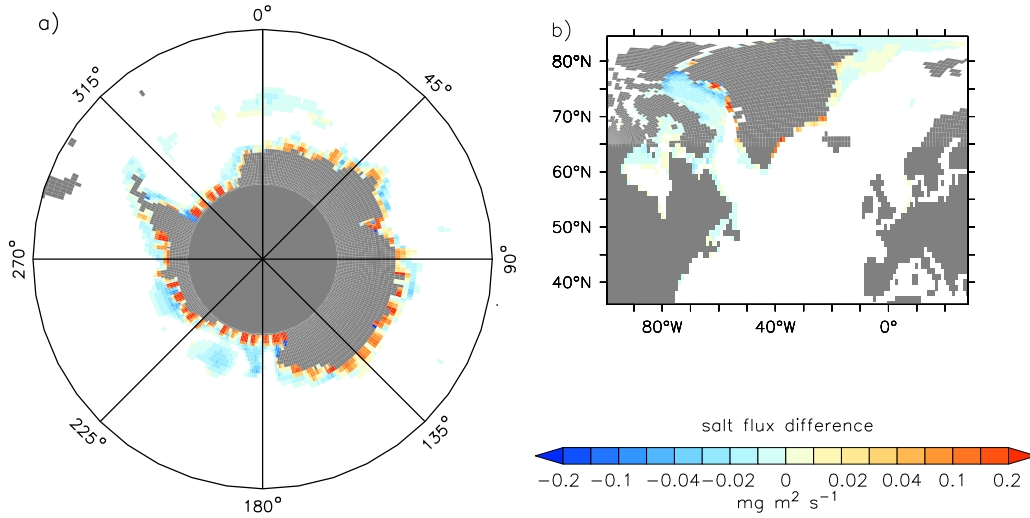


Figure 5: Difference CTRL-BITS of the salt flux from the ocean into sea ice in $10^{-6} \text{ kg m}^2 \text{ s}^{-1}$ for a) the Southern Ocean and b) the North Atlantic based on a 100 year mean. This salt flux is associated with frazil ice formation. Yellow-red colors (positive values) indicate less sea-ice formation in BITS due to redirecting the calving flux which ultimately lead to local sea-ice formation in CTRL, blue colors (negative values) mean more sea-ice formation in BITS where freshening and cooling now prevail due to iceberg melt farther off shore.

locally and further upstream of the Antarctic Coastal Current. The related changes in sea surface salinity (SST) are discussed below.

Changes in in-situ sea-ice thickness are less extensive than changes in sea-ice concentration. Compared to the CTRL experiment sea ice is thinner in the BITS run mostly in places close to major, single discharge points. For example, a plume of thinner sea ice is visible extending from Prydz Bay (75° E), where the Amery Ice Shelf is located (Figure 4d); the same can be seen for major discharge points in the D’Urville Sea or the Haakon VII Sea ($0\text{--}30^\circ \text{ E}$). In the latter, the decrease in thickness is most pronounced with about 0.5 m. More widely spread decreases in sea-ice thickness can also be found in the Weddell, Amundsen, and Bellingshausen seas (Figure 4d). The spreading is caused by a chain of discharge locations along the coast in the respective region.

In the CTRL run, sea ice of extraordinary thickness grows in small (in terms of the 1° resolution of the model grid) semi-enclosed bays because huge amounts of frazil ice are formed when the snow discharge enters an ocean

at the freezing point. Since snow is fresh water and model sea ice has a constant salinity of 5 salt is taken from ambient ocean waters during the formation. Figure 5 depicts the difference in salt uptake by sea ice between runs CTRL and BITS. We can clearly see the discrete snow discharge locations around Antarctica represented by positive differences in Figure 5. The effect is less prominent around Greenland because the discharge volume amounts to only 10% of that of Antarctica. The introduction of icebergs successfully eliminates this false freshening signal in the ocean.

In the BITS experiment a sea-ice thickness increase of 0.5 m based on a 100 year average can be seen in the western Ross Sea (Figure 4d). This can be explained by an accumulation of icebergs in the western corner of the Ross Sea, driven by predominantly onshore and circular wind and ocean current patterns respectively. Their local melt in summer produces a fresh-water lens that initiates stronger sea-ice growth.

In contrast, changes of the sea-ice cover due to the introduction of icebergs are small and local on the northern hemisphere. At the major calving sites along the southeast and west coast of Greenland sea-ice concentration is reduced by up to 10% right at the coast. A significant change in sea-ice thickness was not found on the northern hemisphere.

The decrease in sea-ice mass between the control run and those with icebergs is mainly caused by the redirection of the snow discharge mass. In the CTRL experiment the sea-ice cover benefits from discharging the calving flux right at the coast in winter. The instantaneous frazil formation results in a generally thicker and denser sea-ice cover. A simple calculation based on the scales of the involved mass flux and sea-ice area gives a rough estimate of the impact of redirecting the calving flux: The snow discharge from Antarctica is about $2 \cdot 10^{15}$ kg yr⁻¹. Distributing this mass over the entire southern hemisphere sea ice area, which is of the order of 10^{13} m², and assuming a sea-ice density of 900 kg m⁻³ yields a sea-ice thickness decrease of 0.22 m yr⁻¹. This corresponds to an energy uptake of 2.2 W m⁻² (the latent heat of fusion of water is $334 \cdot 10^3$ J kg⁻¹). For comparison, in a climate scenario with doubled atmospheric CO₂ the global radiative forcing is about 4 W m⁻² (Meehl et al., 2007, Tab. 10.2).

3.4. Ocean

3.4.1. Surface properties

The reduced sea-ice concentration in the experiments with icebergs results in a warming of the ocean due to greater radiative absorption leading to an

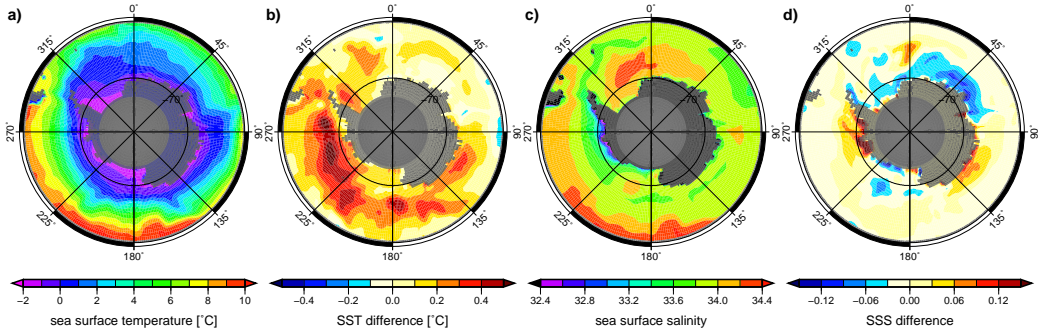


Figure 6: 100 year averages of sea surface properties and their change due to the introduction of icebergs. a) Sea surface temperature (SST) in $^{\circ}\text{C}$ in CTRL. b) SST difference in $^{\circ}\text{C}$ of BITS-CTRL. c) Sea surface salinity (SSS) in CTRL. d) SSS difference of BITS-CTRL.

423 increase of SST (see Figure 6). This summer effect dominates the presented
 424 annual mean SST over any sea-ice mass gain from enhanced freezing during
 425 winter. The warming of the ocean surface is most prominent in the Pacific
 426 sector of the Southern Ocean with an increase of up to 0.5°C . Its center is
 427 roughly located at the sea-ice edge (cf. Figures 4b and 6b). In contrast, a
 428 few locations with slight cooling can be found in the Atlantic and western
 429 Indian Ocean sectors. The warming and cooling patterns correlate with
 430 the distribution of sea-ice concentration decrease and increase, respectively,
 431 depicted in Figure 4b.

432 The differences in the sea surface salinity (SSS) between the CTRL and
 433 BITS experiments is more diverse. The magnitudes of freshening and salin-
 434 ization are the same with values of up to 0.2. Surface waters become more
 435 saline in the Amundsen and Bellinghausen seas, and in the D’Urville Sea. A
 436 wide area of freshening is located in the Atlantic and Indian Ocean sectors.
 437 Also the Ross Sea area is fresher in the BITS run. Here, the fresh-water
 438 lens addressed earlier in conjunction with the sea-ice thickness changes is
 439 visible (dark blue spot in the very southwestern corner of the Ross Sea in
 440 Figure 6d) with an overall extreme difference of -1.37 at 74.2°S . In general,
 441 changes in salinity can be attributed to the changed spatial distribution of
 442 frozen fresh-water discharge to the ocean in the iceberg experiments. How-
 443 ever, mechanisms leading to changes in SSS are complex and involve ocean
 444 circulation and sea-ice melt, too. For instance, the ocean is saltier in BITS
 445 where a large calving flux initiates frazil-ice growth in CTRL, which is asso-
 446 ciated with a reduction of the ocean salinity because the calving flux is fresh
 447 and sea ice has an assigned constant salinity in the CGCM (Figure 6). The

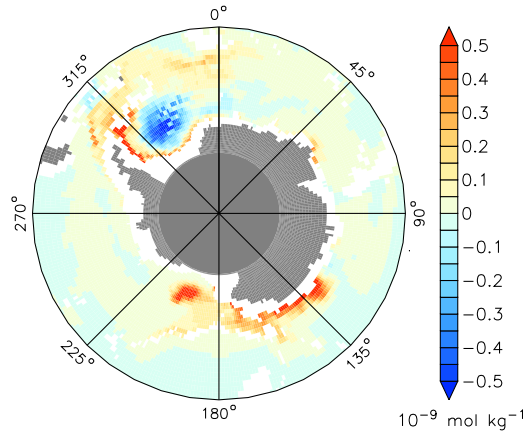


Figure 7: Annual average of the CFC-11 concentration differences BITS-CTRL in mol kg^{-1} in the Southern Ocean at 3000 m depth of model year 120, 31 years after tracer release at the surface. The CFC tracer emphasizes continental-shelf convection in the Weddell and Ross seas, which are strongly increased in the iceberg experiments (positive differences). The impact of an event of strong open ocean convection in the Weddell Sea in CTRL can also be seen (negative differences). Regions of water depths of less than 3000 m are white.

448 reduction in sea-ice mass due to a redirected calving flux results in a reduced
 449 freshwater input to the ocean from sea-ice melt leading to greater SSS in
 450 BITS (cf. Figures 4d and 6d around 0° longitude). The widespread fresh-
 451 ening in BITS in the Atlantic and Indian Ocean sectors, which stimulates
 452 sea-ice growth (Figure 4b), originates from an accumulation of iceberg melt
 453 water in this region. This is favored by a strong southward component of
 454 the Antarctic Coastal Current in this region (not shown) and major calving
 455 sites upstream, such as the Amery Ice Shelf.

456 3.4.2. Deep convection

457 In the CTRL experiment the snow discharge enters the ocean directly at
 458 the coast while in the BERG and BITS experiments icebergs transport this
 459 fresh water away from the coast. Exporting this fresh water off the conti-
 460 nental shelf regions enhances the formation of dense waters in these areas,
 461 which in turn encourages deep convection at the shelf break in particular in
 462 the Weddell and Ross seas. The resulting increase in downslope flow at the
 463 shelf break is visualized in Figure 7 in terms of the CFC-11 tracer concentra-
 464 tion. Along the shelf break in the Weddell Sea and west of the Ross Sea the
 465 CFC-11 concentration is up to $1 \times 10^{-9} \text{ mol kg}^{-1}$ higher in BITS compared

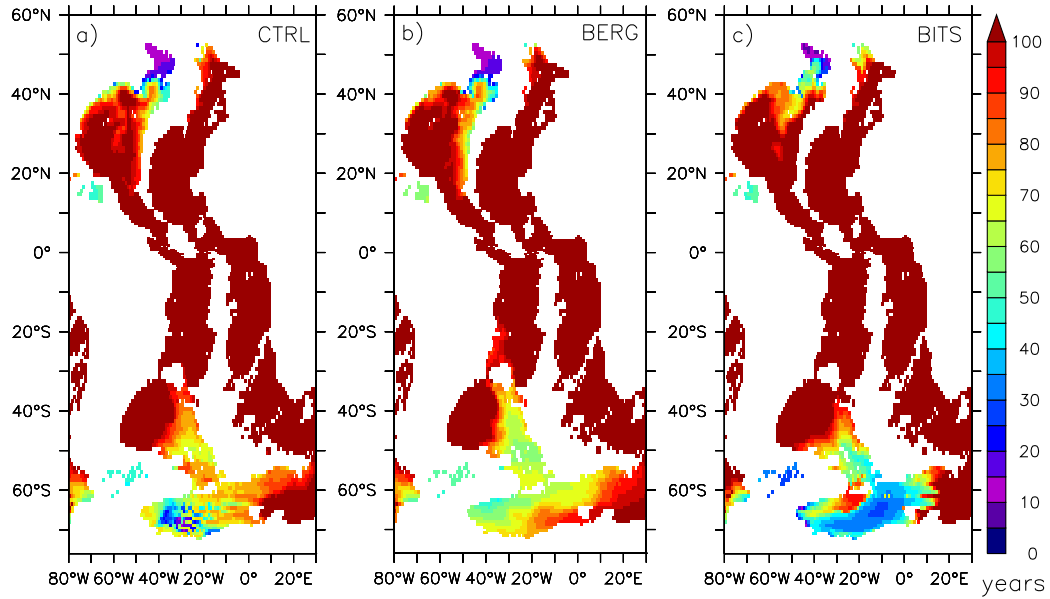


Figure 8: Ideal age tracer of ocean waters in the Atlantic Ocean at 4200 m depth in years for a) CTRL, b) BERG, and c) BITS. The annual average of model year 120 is shown.

to CTRL at a depth of about 3000 m 31 years after the tracer has been released at the surface in model year 89. This is an increase by a factor of 2–3. At this time the CFC-11 concentration reaches $1\text{--}1.5 \times 10^{-9} \text{ mol kg}^{-1}$ along the shelf break in the BITS experiment (not shown). Figure 7 also depicts the effect of an event of strong open ocean convection in CTRL in the central Weddell Sea. Due to the deep mixing the CFC-11 concentration is up to $0.5 \times 10^{-9} \text{ mol kg}^{-1}$ greater than in BITS, where it amounts to only $0.1 \times 10^{-9} \text{ mol kg}^{-1}$.

The enhanced ventilation of deep waters with the help of icebergs can also be deduced from an ideal age tracer, which simply counts the years since the last contact of water masses with the ocean surface. Figure 8 shows the results of all three experiments for the Atlantic Ocean at a depth of 4200 m. To begin with, we demonstrate the effect of the icebergs by comparing the spatial extent of the 70 year isochrone (yellow in Figure 8). In BERG the younger waters reach farther north and east from the Weddell Sea than in CTRL, reaching 39° S and 8° E , respectively, compared to only 47° S and 5° W , respectively. In BITS this extent is not much increased but waters are much younger. Apart from the strong effect of the open ocean convection in

CTRL mentioned above, the water age does not fall below 50 years in CTRL and BERG in the South Atlantic, whereas BITS results in waters younger than 30 years at this depth. This emphasizes the importance of transporting the calving flux away from coastal and shelf regions, in which the additional bergy bits are obviously more effective.

Although the open ocean convection in CTRL also allowed waters younger than 40 years to penetrate to greater depth in the central Weddell Sea (Figure 8a) it is important to enable CGCMs to produce deep waters on the continental shelf. This process, also referred to as the continental shelf pump, is expected to have a stronger impact on the carbon budget of the climate system than open ocean convection (Tsunogai et al., 1999). Carbon solubility depends strongly on the temperature of the water. On shallow shelves the water can cool down much more than in the open ocean and hence dissolve more CO₂. Additionally, the residence time at the surface of water on the shelf is longer, which also allows an increased uptake of carbon compared to the open ocean. The release of oxygen to the atmosphere happens much faster than the uptake of carbon. Hence, water originating from shelf convection has a greater carbon to oxygen ratio than water from open ocean convection. Considering the estimate of Tsunogai et al. (1999) we conclude that it is important to simulate the convection mechanisms correctly in a CGCM, which is used for ecosystem studies. The icebergs, and in particular the bergy bits, help to strengthen the continental shelf pump.

Comparing the CTRL and BERG results in Figures 8a and 8b, respectively, the icebergs seem to have less impact on the age structure of the deep water in the North Atlantic but result in an increase in the amount of younger waters, which are less than 70 years old. It is noteworthy that the pathway of the deep water changes in the BITS experiment (Figure 8c), which no longer flows along the Mid Atlantic Ridge but heads southward in the center of the basin.

4. Discussion

4.1. Comparison to previous model studies and observations

A correctly simulated calving flux is a necessary precondition in order to achieve a natural distribution of iceberg mass on the ocean. In the absence of an ice-shelf model we use the snow discharge generated by the CGCM as input for the iceberg simulation. Observational estimates of the calving flux have a rather wide range. Jacobs et al. (1992) list estimates of nine

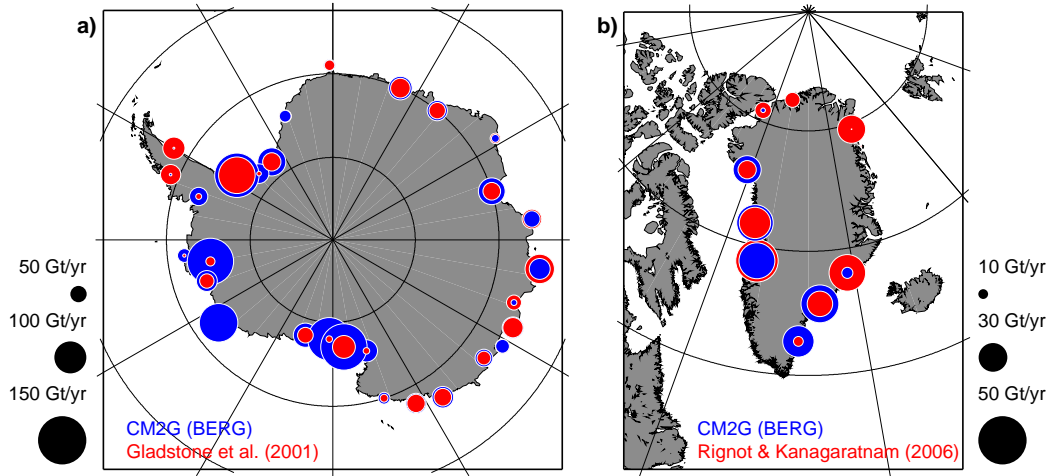


Figure 9: Comparison of simulated (blue, from experiment BERG) and observed calving rates (red). a) 29 calving locations around Antarctica given by Gladstone et al. (2001). b) Glacial discharge published by Rignot and Kanagaratnam (2006) concentrated in 9 main regions.

520 different studies, including their own, ranging from 855 to 2400 Gt yr⁻¹
 521 , averaging at 1753 Gt yr⁻¹ for Antarctica. Gladstone et al. (2001) made
 522 a very comprehensive approach to provide a climatological calving rate of
 523 1332 Gt yr⁻¹ for their iceberg model study. More recently Hooke (2005)
 524 stated a calving flux of 2072 ± 304 Gt yr⁻¹ for Antarctica and 235 ± 33 Gt yr⁻¹
 525 for Greenland. For their model study Bigg et al. (1997) derived a mass flux of
 526 218 Gt yr⁻¹ from Greenland. And most recently Rignot and Kanagaratnam
 527 (2006) calculated Greenlandic glacier flow speeds from remote sensing data
 528 yielding a calving rate of 291 Gt yr⁻¹. A source of uncertainty, in particular
 529 for the Antarctic, is the unknown ratio of ice-shelf bottom melt and calving.
 530 Both play an important role in the mass balance of the Antarctic ice sheet and
 531 their ratio differs from site to site (Lemke et al., 2007). Within these limits
 532 the agreement of our modeled and the observed calving fluxes is very good.
 533 The Greenlandic calving flux in our model amounts to 210 Gt yr⁻¹. Here,
 534 it should be kept in mind that Rignot and Kanagaratnam (2006) account
 535 for the recent increase in flow speed of the glaciers, i.e. our model better
 536 matches a climatological mean. With an average calving rate of 2000 Gt yr⁻¹
 537 from Antarctica our model is close to the average calving estimates (Jacobs
 538 et al., 1992; Hooke, 2005) but produces 50% more iceberg mass per year
 539 than Gladstone et al. (2001) prescribed in their model study. This needs to

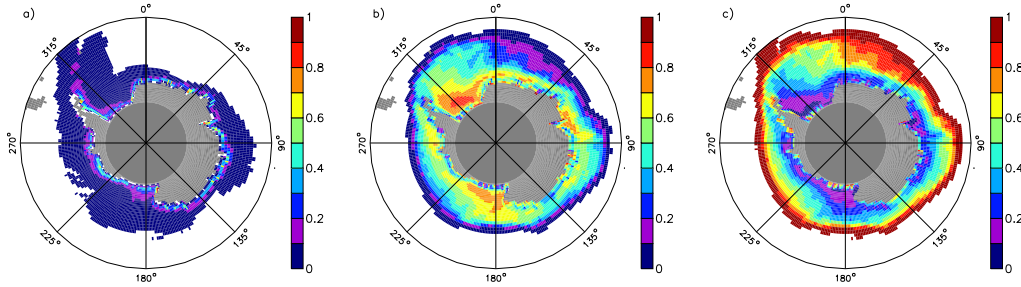


Figure 10: Partitioning of the fresh-water flux entering the Southern Ocean: a) fraction of iceberg melt, b) fraction of sea-ice melt, and c) fraction of precipitation including liquid runoff. Results of the BITS experiment are shown. In panels a and b white areas indicate values falling below 0.005, in panel c this marks values greater than 0.995.

540 be considered when comparing the melt water distribution in the Southern
 541 Ocean to Gladstone et al. (2001) and Silva et al. (2006).

542 Iceberg calving rate estimates at individual locations are provided by
 543 Gladstone et al. (2001) and Rignot and Kanagaratnam (2006) for Antarctica
 544 and Greenland respectively. In Figure 9 we present the calving flux from the
 545 BERG experiment averaged over 100 years together with these data. Our
 546 model has 88 discharge points around Antarctica but Gladstone et al. (2001)
 547 chose only 29 calving sites. For this comparison, not for the experiments,
 548 we concentrated the modeled flux at the locations of Gladstone et al. (2001)
 549 combining catchment basins of the model to resemble those of the observa-
 550 tions. We also merged the data of 32 individual Greenlandic glaciers given
 551 by Rignot and Kanagaratnam (2006) and the 24 discharge locations around
 552 Greenland of the CGCM into 9 calving sites to achieve best overlap of the
 553 catchment basins and pronounce the major iceberg formation areas. From
 554 the maps in Figure 9 we can see that the calving flux in our simulations has
 555 a realistic spatial distribution, i.e. there are distinct maxima at locations of
 556 large ice shelves and glaciers around Antarctica and Greenland respectively.
 557 The difference in total calving between Gladstone et al. (2001) and our model
 558 is mostly due to an overestimation by the model in the Ross, Amundsen, and
 559 Bellinghausen seas (Figure 9a). In a future version of the CGCM this could
 560 be changed by dividing the snow discharge between calving and ice-shelf bot-
 561 tom melt. Ice-shelf bottom melt is particularly strong in the Amundsen and
 562 Bellinghausen seas (Rignot and Jacobs, 2002). In the case of Greenland the
 563 spatial distribution of the simulated calving flux compares well with the ob-
 564 servations of Rignot and Kanagaratnam (2006), in particular along the west

565 coast of Greenland (Figure 9b).

566 It is important to note that the major impact of the icebergs on the
567 coupled system is the effective transport of fresh water away from the shelf
568 regions. As Figure 10a shows, iceberg melt water rarely accounts for more
569 than 10% of the total fresh-water input to the open ocean in our experiments,
570 i.e. the fresh water released by the icebergs barely affects the ocean’s strati-
571 fication in these regions. In contrast, in coastal areas iceberg melt accounts
572 for up to half of the fresh-water input. Hence, large icebergs that survive
573 several melt seasons and drift farther away from the coast have the greatest
574 impact on the freshwater balance. In contrast, a transport of the calving
575 flux with sea ice, as apparently happens in CTRL, where the snow is quickly
576 turned into frazil ice and further enhancing sea-ice thickness, is less effective,
577 because sea-ice melt dominates the freshwater flux into the ocean in partic-
578 ular on the continental shelves in the Weddell and Ross seas (Figure 10b).
579 Silva et al. (2006) estimated that about half of the total meltwater flux from
580 icebergs in the Southern Ocean is related to giant icebergs, icebergs that ex-
581 ceed 8 km in length, which are not yet considered in our model. The authors
582 also showed that these giant icebergs can reach farther north than those we
583 simulate here. Gladstone et al. (2001) found that iceberg melt rarely reaches
584 the same magnitude as precipitation but does so for instance in coastal areas
585 in the Weddell Sea, which agrees with our results (Figures 10a and 10c).

586 Forming icebergs from the snow discharge has a strong impact on the com-
587 pactness and thickness of the sea-ice cover in the Southern Ocean. However,
588 the simulated sea-ice extent (total area within the 15% isoline) is mostly un-
589 affected (Figure 4b). With 15.3×10^6 km² the model’s sea-ice extent exceeds
590 the observed long-term (1979–2006) average of 11.5×10^6 km² (Cavalieri and
591 Parkinson, 2008) by one-third. In contrast, the simulated mean sea-ice area,
592 which considers the fractional area covered by sea ice, is smaller ranging be-
593 tween 7.0×10^6 km² (BERG and BITS) and 7.4×10^6 km² (CTRL) compared
594 to the observed 8.7×10^6 km² (Cavalieri and Parkinson, 2008). This clearly
595 shows the low compactness of the southern hemisphere sea ice in our CGCM
596 results. Furthermore, the annual mean sea-ice thickness is too thin. In the
597 CTRL experiment, which has generally thicker sea ice than the runs with
598 icebergs, the ice is about 0.2 to 0.5 m thinner than observed (Worby et al.,
599 2008) in many locations, in particular (far) off the coast. The underestima-
600 tion is greater in those regions where thicker ice occurs in both, model and
601 data. The simulated sea-ice cover of the CTRL experiment is thicker than
602 observed where ice growth is forced by the snow discharge from land. The

603 smaller sea-ice mass in our model can be attributed to the generally warmer
 604 surface ocean south of 50°S . The CTRL run has a SST warm bias of about
 605 2°C on average in this region (results shown in Figure 6a compared to a 20
 606 year composite of observed SST from Reynolds et al. (2002)). Discharging
 607 snow in winter and hence into a cold ocean in the CTRL experiment results
 608 in an extensive frazil ice formation, which makes the sea ice more resistive to
 609 melting by significantly increasing its thickness (see above) and hence partly
 610 compensates the impact of warm SSTs. We found that enhanced growth in
 611 winter, as a result of a generally thinner and less compact sea-ice cover in
 612 experiments BERG and BITS, cannot compensate for the additional melt
 613 in summer caused by a reduction in surface albedo due to the same sea ice
 614 changes. In summer the ocean gains more heat due to open water areas
 615 within the ice cover enhancing the warm bias the model has in the Southern
 616 Ocean (Figure 6b).

617 The reduced compactness of the sea-ice cover in the experiments with
 618 icebergs unintentionally affects the lifetime of the icebergs. The dominant
 619 iceberg melt parametrization, the wave erosion, is moderated by sea-ice con-
 620 centration because the ice cover damps waves. The changes in sea ice between
 621 runs with icebergs and without are mainly a result of the redirection of the
 622 snow discharge and to a lesser degree due to the meltwater distribution of
 623 the icebergs.

624 In general, the effect of icebergs in a CGCM strongly depends on how the
 625 control run deals with the excess snow runoff. While the runoff enters the
 626 ocean directly at the coast in CTRL, Jongma et al. (2009) chose the opposite
 627 approach: a homogeneous redistribution to the Ocean south of 55°S . As we
 628 mentioned in the introduction they performed a similar study but prescribed
 629 the calving flux. In Jongma et al. (2009) the additional fresh water in polar
 630 waters from iceberg melt enhances stratification which in turn stimulates
 631 sea-ice formation. The authors also found an increase in the production of
 632 AABW of 1–2 Sv due to the freshening and cooling effect of iceberg melt.
 633 In our experiments BERG and BITS the AABW production is greater than
 634 in CTRL by 1 Sv at 60°S . This change is about 10% of the total AABW
 635 production in CTRL, which also agrees well with the results of Jongma et al.
 636 (2009).

637 The snow discharge from the continents may be small compared to other
 638 sources of fresh water entering the ocean, but where and when the calving
 639 flux enters the ocean matters. It should be noted here, that in all our ex-
 640 periments the liquid runoff is greater than the snow discharge throughout

641 the year, which means that the ability of the icebergs to reduce the fresh-
 642 water bias in coastal waters, in particular around Antarctica, is limited. In
 643 order to reduce computational costs the explicit iceberg simulation could be
 644 replaced by an invariant distribution pattern. This distribution could be de-
 645 rived from a long-term average, e.g. over 100 years, of the iceberg melt water
 646 distribution of experiments such as BERG or BITS. This approach is along
 647 the lines of Gordon et al. (2000) but would improve the redistribution pat-
 648 tern to match the individual CGCM's climate and climate change response.
 649 Applying the iceberg melt water pattern could also change the results of so-
 650 called waterhosing experiments because the typically used release pattern of
 651 the additional fresh water differs from that of iceberg melt presented here
 652 (cf. Figure 2 with Gerdes et al. (2006, Fig. 3) or Stammer (2008, Fig. 1)).

653 *4.2. Shortcomings of the current model*

654 The iceberg model we use in this study has certain shortcomings, which
 655 are partly due to simplifications that were necessary to realize this study
 656 with the CGCM CM2G and partly caused by limited knowledge on related
 657 processes in nature. In the following we will briefly discuss most of these
 658 issues. For all of these we seek solutions, but the time scale is beyond this
 659 study. The expected impact of the various missing processes on the CGCM
 660 result differs.

661 Currently iceberg calving is initiated by splitting the snow discharge into
 662 ten iceberg size categories. There are two caveats regarding this step function,
 663 which we adopted from Gladstone et al. (2001): First, the first bin is the
 664 major mode of the distribution (see last column of Table 1) and represents
 665 all icebergs that are smaller than 60 meters in length, i.e. they are of the
 666 same size as our bergy bits. This means that the first bin of the distribution
 667 includes brash ice, which should not be considered an iceberg but can be
 668 assumed to melt locally or be enclosed by sea ice. We conclude that the
 669 initial length of icebergs should not fall below 100 m or 200 m. This is
 670 supported by recently published observations that icebergs less than 100 m
 671 long account for only 1% of the reported iceberg volume (Jacka and Giles,
 672 2007). Second, the frequency distribution of Gladstone et al. (2001) is derived
 673 from ship observations and therefore represents icebergs in a state of decay
 674 rather than their original size at the calving site. Applying a continuous
 675 iceberg size distribution in conjunction with a random number simulator to
 676 the calving problem would be an obvious alternative.

677 A step further would be to include giant icebergs in the simulation, i.e. ice-
678 bergs exceeding 8 km in length. Silva et al. (2006) showed the importance
679 of these large icebergs, which account for half of the fresh-water flux re-
680 leased from icebergs and melt farther away from the shelf area surviving
681 much longer in or across the Antarctic Circumpolar Current. However, such
682 giant icebergs do not calve regularly but result from great ice-shelf break-up
683 events and are thus not easy to parameterize. There is no immediately ob-
684 vious solution to implement giant icebergs in a CGCM because on the one
685 hand a prescribed calving such as in Silva et al. (2006) reduces the freedom
686 of the CGCM and on the other hand the calving process as it is presently
687 understood is too complex for a CGCM suitable parameterization even with
688 a coupled ice-sheet model available.

689 All of the snow discharge is currently used to form icebergs. However,
690 parts of it could or should enter the ocean via ice-shelf bottom melt. In
691 order to realize this, some representation of ice-shelf cavities needs to be
692 introduced to the CGCM. Although iceberg calving and ice-shelf bottom
693 melt have been identified as the major pathways for mass loss of the great
694 ice sheets (Lemke et al., 2007) the ratio between these two is still under
695 discussion as measurements or estimates of ice-shelf bottom melt are rare
696 but their number and quality is increasing.

697 For this study the maximum thickness of icebergs at the moment of
698 calving is set to 250 m following Gladstone et al. (2001). However, the
699 initial thickness should be a function of the average thickness of the ice
700 shelf or glacier that the iceberg originates from and also depend on the local
701 bathymetry used in the CGCM.

702 To this point we consider grounding of icebergs only partially. Icebergs
703 may run aground in two different ways. Horizontally, they may interact with
704 the coast, and vertically they can ground in shallow areas of the continental
705 shelf (Bigg et al., 1997). The former is included in our model and allows
706 the icebergs to creep along the coast, i.e. we consider only the displacement
707 of the Lagrangian particle that is parallel to the coast whenever an iceberg
708 hits land. Including the latter requires a reasonable bathymetry. Allowing
709 larger icebergs that approach the continental shelf from deeper waters and
710 that greatly exceed the water depth on the shelf to creep along the shelf edge
711 like along a coastline could strengthen the impact of the icebergs because it
712 would prevent them from melting on the continental shelf. This could, in
713 particular, impact the Weddell Sea where icebergs enter from the east and
714 leave to the north with the gyre current.

715 We also did not consider interactions between icebergs themselves. Colli-
716 sions may become a major force, in particular in coastal regimes (MacAyeal
717 et al., 2008). In the presence of sea-ice concentrations exceeding 85% or 95%
718 icebergs may get locked into the dense sea-ice cover (Lichey and Hellmer,
719 2001; Schodlok et al., 2006). However, sea ice may not always act as a col-
720 lector of the wind momentum (Aoki, 2003). The locking of icebergs has
721 been simulated by Lichey and Hellmer (2001) with an un-coupled large-scale
722 sea-ice model in a discontinuous manner. A possibility to force the coherent
723 motion of icebergs and sea ice would be to use a variable sea-ice drag coef-
724 ficient in the momentum balance of the icebergs, which grows exponentially
725 with sea-ice concentration.

726 Although the individual weight of the icebergs imposes a pressure on the
727 ocean in our model the Lagrangian particles do not cover any area but are
728 simply points in space on the Eulerian grid of the CGCM. Considering an
729 areal extent of the icebergs would be most important for the global albedo
730 because icebergs often have a brighter surface than their surroundings, in
731 particular in open water.

732 A major simplification in our model is that icebergs interact only with
733 the surface layer of the ocean. As icebergs may penetrate the ocean to
734 depths of several hundred meters the iceberg model would need the full 3-D
735 fields of ocean temperature and current speeds to better reflect reality. The
736 exchanged fresh-water field would need to become a 3-D array, too, because
737 the melt water is naturally not only entrained in the surface layer as is the
738 case in the current model. Both, the dynamic interaction of a full 3-D iceberg
739 body and the release of fresh water at depth would then affect the ocean's
740 stratification. The associated small-scale turbulence in the surroundings of
741 the iceberg might enhance mixing over greater depths but will need to be
742 parameterized. However, the overall impact of this simplification is limited
743 because the dominant melt term in the mass balance of the icebergs, wave
744 erosion, is a surface process.

745 Finally, the model lacks the true time scale of an ice sheet though our
746 approach includes a buffer, which de-couples the seasonal cycles of snow fall
747 over the continent and fresh-water discharge to the ocean (Figure 1). Hence,
748 for climate change scenarios a change in iceberg calving indicates rather a
749 change in precipitation over ice covered land masses than a change of ice-
750 sheet or ice-shelf behaviour. Nevertheless, a generally warmer ocean in a
751 climate change scenario strongly impacts the iceberg melt behaviour and the
752 iceberg mass accumulated on the ocean.

5. Conclusions

We have shown that the parameterization of the frozen fresh-water flux from land to ocean with simplified Lagrangian icebergs can successfully be applied in a fully coupled model environment. The new parameterization is a more realistic closure of the fresh-water cycle at the land-ice ocean interface because it considers the dynamic and thermodynamic processes—transport and slow melt—related to the discharge of frozen water. Icebergs are, besides ice-shelf bottom melt, the major pathway for ice-sheet mass loss. In contrast to any prescribed fresh-water distribution the fully coupled icebergs allow the model to freely develop the balance between precipitation, calving, and melt water flux as well as the forcing of melt processes, such as ocean temperature and wind speeds.

We found that the implementation of icebergs into a CGCM importantly affects the timing and spatial distribution of the melt water flux. The snow discharge is greatest during the winter season whereas iceberg melt peaks in summer. Furthermore, the spatial distributions of iceberg mass and melt water have a strong gradient perpendicular to the coast with decreasing magnitude towards the open sea. Both aspects, time and location, importantly affect the sea-ice cover and dense water formation. The sea-ice cover is thinner and less compact with icebergs compared to the control experiment. In the latter the snow discharge enters the ocean at the coast, stimulating sea-ice growth. In contrast, Jongma et al. (2009) report a sea-ice growth enhancing effect of the iceberg melt water because in their control experiments the authors either neglect snow discharge or redistribute the associated freshwater homogeneously over the Southern Ocean area. Hence, we conclude that the handling of the snow discharge in coupled models is important for biases without icebergs.

In our experiments the reduced fresh-water input over continental shelf regions in experiments with icebergs and in particular with bergy bits enhances the deep and bottom water formation. This change is strongest in the Weddell and Ross seas. We find a 10% increase (1 Sv) of AABW production, which agrees well with Jongma et al. (2009). We found that similarly dense waters may form in the control experiment but these are due to open water convection in contrast to the enhanced shelf convection in the iceberg experiments. The distinction between these formation processes has significant implications for biogeochemical processes, particularly for carbon uptake.

In general, the impact of introducing icebergs are much greater on the

southern than on the northern hemisphere, because about 90% of the global iceberg mass originates from Antarctica. In the northern hemisphere most icebergs originate from Greenland, where glaciers calve into the Greenland and Labrador seas. Hence, the Arctic Ocean and its sea-ice cover are not significantly affected. The deep-water formation in the North Atlantic depends more on cooling of the surface ocean by winds than on salinization by sea-ice formation and therefore the icebergs have a much weaker impact than in the Weddell or Ross seas.

Despite known shortcomings the iceberg parameterization as described here will be used at GFDL in model scenarios for the next IPCC Assessment Report. The development of an ice-sheet model to be coupled to the CGCM will offer new opportunities to better simulate iceberg and ice-shelf bottom melt processes. The introduction of freely evolving icebergs in a CGCM also opens up possibilities in palaeoclimate simulations (e.g. Wiersma and Jongma, 2009) or biogeochemical model studies. For instance, it has been shown that icebergs play a role in the ecosystem of the (sub-)polar oceans (e.g. Raiswell et al., 2008; Lancelot et al., 2009). The release of sediments, namely iron during iceberg melt stimulates phytoplankton growth.

Acknowledgements

We thank Stephen Griffies, Bob Hallberg and Mike Winton for valuable discussions. This study was inspired by results obtained by Eric Galbraith who was experimenting with distributing the calving over the open ocean away from the coasts in a low resolution coupled model. We also like to thank NOAA/GFDL for providing the computational infrastructure to run the CGCM experiments. This report was prepared by Torge Martin under award NA17RJ2612 and NA08OAR4320752 from the National Oceanic and Atmospheric Administration, U.S. Department of Commerce. The statements, findings, conclusions, and recommendations are those of the authors and do not necessarily reflect the views of the National Oceanic and Atmospheric Administration, or the U.S. Department of Commerce.

Appendix A. Iceberg model equations

The motion of fluids in a CGCM are generally described from an Eulerian point of view. In contrast, we treat icebergs as Lagrangian objects, which are considered points in space. The present model mainly resembles that of Bigg

et al. (1997) and Gladstone et al. (2001) though deviating in some aspects. Physically reasonable modifications proved to enhance numerical stability of the model. Most notably, we revised the formula of the wave radiation force.

Icebergs are approximated as cuboids with total thickness T , length L and width W . This simplifies the calculation of the different working surfaces in the momentum and mass balance equations. The total thickness is divided into freeboard F , which is height above water level, and draught D , the submerged depth of the iceberg, with $T = F + D$ and $D = \rho/\rho_o T \simeq 0.8 T$. Here, we assume an average density of $\rho = 850 \text{ kg m}^{-3}$ for all icebergs (Silva et al., 2006) and an average density of seawater $\rho_o = 1025 \text{ kg m}^{-3}$.

The momentum balance for an iceberg of mass M is given by

$$M \frac{d\vec{v}}{dt} = -M f \times \vec{v} + \vec{\tau}_a + \vec{\tau}_o + \vec{\tau}_i + \vec{F}_r + \vec{F}_p \quad (\text{A.1})$$

where $d/dt = \partial/\partial t + \vec{\nabla} \cdot \vec{v}$ is the absolute derivative in time and f denotes the Coriolis parameter. The momentum balance comprises drag forces for atmosphere, ocean and sea ice:

$$\vec{\tau}_a = \rho_a (0.5 c_{a,v} W F + c_{a,h} L W) |\vec{v}_a - \vec{v}| (\vec{v}_a - \vec{v}) \quad (\text{A.2a})$$

$$\vec{\tau}_o = \rho_o (0.5 c_{o,v} W (D - T_i) + c_{o,h} L W) |\vec{v}_o - \vec{v}| (\vec{v}_o - \vec{v}) \quad (\text{A.2b})$$

$$\vec{\tau}_i = \rho_i 0.5 c_{i,v} W T_i |\vec{v}_i - \vec{v}| (\vec{v}_i - \vec{v}) \quad (\text{A.2c})$$

where indexes a , o and i refer to atmosphere, ocean and sea ice, respectively, ρ_x with $x = \{a, o, i\}$ denotes density, and $c_{x,v}$ and $c_{x,h}$ are the associated vertical and horizontal drag coefficients. Following Gladstone et al. (2001) we set $c_{a,v} = 1.3$, $c_{a,h} = 0.0055$, $c_{o,v} = 0.9$, and $c_{o,h} = 0.0012$. Sea ice acts only on the side walls of the iceberg, playing a minor roll because its thickness T_i is much smaller than D for most of the iceberg's lifetime. The drag coefficient $c_{i,v}$ is assumed to equal $c_{o,v}$. The respective working surfaces were not explicitly mentioned by Bigg et al. (1997) and Gladstone et al. (2001) and thus may be different here.

The iceberg is further driven by the wave radiation force

$$\vec{F}_r = \frac{1}{2} \rho_o c_r g a \min(a, F) \frac{2 L W}{L + W} \frac{\vec{v}_a}{|\vec{v}_a|} \quad (\text{A.3})$$

where g is the acceleration due to gravity and a denotes the wave amplitude, which is empirically related to the wind speed. Here, we considerably deviate from the studies of Bigg et al. (1997) and Gladstone et al. (2001) as we

- 851 (1) consider only the wind speed relative to the ocean current in the equa-
 852 tion for the wave amplitude $a = 0.010125 |\vec{v}_a - \vec{v}_o|^2$, while we still as-
 853 sume that surface waves travel in the same direction as the wind,
- 854 (2) consider that the wave radiation force decreases when the freeboard of
 855 the iceberg F becomes smaller than the waves ($F < a$),
- 856 (3) account for a varying ratio of the length L and width W of the icebergs
 857 by using the harmonic mean of L and W , which varies between W and
 858 $2W$, in the determination of the working surface, and
- 859 (4) apply a variable coefficient c_r that damps the wave radiation force when
 860 the ratio of iceberg length and wavelength becomes small. We defined
 861 the wave radiation coefficient c_r as

$$c_r = 0.06 \min \left(\max \left[0, \frac{L - L_c}{L_t - L_c} \right], 1 \right) \quad (\text{A.4})$$

862 where the cutoff length $L_c = 0.125 L_w$ and the upper limit $L_t = 0.25 L_w$
 863 are chosen to resemble the curve presented by Carrieres et al. (2001,
 864 their Fig. 6) with the wavelength empirically derived from $L_w =$
 865 $0.32 |\vec{v}_a - \vec{v}_o|^2$.

866 We found the above changes to be important in stabilizing the model as the
 867 wave radiation force can become the dominant driving force.

868 Finally a pressure gradient force is considered

$$\vec{F}_p = -Mg\vec{\nabla}\eta \quad (\text{A.5})$$

869 that includes the effect of the sea surface slope η to the momentum balance
 870 of the icebergs.

871 The mass balance of an iceberg is given by

$$\rho \frac{d(L W T)}{dt} = \rho (-L W M_b - T (L + W) (M_e + M_v)). \quad (\text{A.6})$$

872 Gladstone et al. (2001) stated that the melt and erosion of an iceberg are
 873 mainly driven by bottom melt M_b , wave erosion M_e and buoyant convection
 874 at the side walls M_v and that all other effects are negligible small. Therefore,
 875 we focused on these three effects. Again, the above equation may be different
 876 from the approaches of Bigg et al. (1997) and Gladstone et al. (2001) with

877 respect to the working surfaces applied. All melt terms have units of meters
878 per day.

879 At the base of an iceberg, turbulence is created by the relative motion of
880 the water passing the iceberg. Since the effective iceberg temperature \tilde{T} is
881 assumed to be constantly at -4°C (Løset, 1993) this turbulence generates a
882 heat flux to the iceberg. The associated melt rate is estimated by

$$M_b = 0.58 |\vec{v} - \vec{v}_o|^{0.8} \frac{\tilde{T}_o - \tilde{T}}{L^{0.2}} \quad (\text{A.7})$$

883 where \tilde{T}_o is the sea surface temperature.

884 The reduction in iceberg volume due to wave erosion is assumed to be
885 directly proportional to the sea state S_s and the sea surface temperature \tilde{T}_o ,
886 which always has a positive impact because $\tilde{T}_o > \tilde{T}$,

$$M_e = \frac{1}{12} S_s (1 + \cos [\pi A_i^3]) (\tilde{T}_o + 2). \quad (\text{A.8})$$

887 However, wave erosion decreases with increasing sea-ice coverage because
888 an ice cover damps waves and reduces the wind fetch. Therefore, Gladstone
889 et al. (2001) included a dependence on the fractional sea-ice area A_i . The
890 above empirical function of wave erosion includes calving of slabs from the
891 iceberg (Bigg et al., 1997). We estimate the sea state by a fit to the Beaufort
892 scale:

$$S_s = \frac{3}{2} |\vec{v}_a - \vec{v}_o|^{1/2} + \frac{1}{10} |\vec{v}_a - \vec{v}_o|. \quad (\text{A.9})$$

893 The permanent temperature contrast between the iceberg and the ocean
894 results in buoyant convection along the side walls of the iceberg. The related
895 heat transfer is a non-negligible contributor to the reduction of iceberg mass.
896 The melt rate of this process was empirically estimated to be

$$M_v = 7.62 \times 10^{-3} \tilde{T}_o + 1.29 \times 10^{-3} \tilde{T}_o^2 \quad (\text{A.10})$$

897 by El-Tahan et al. (2001).

898 Like Bigg et al. (1997) we apply the empirical criterion of Weeks and
899 Mellor (1978)

$$L < \sqrt{0.92 D^2 + 58.32 D} \quad (\text{A.11})$$

900 to allow icebergs to roll over. In this case W and T are instantaneously
901 swapped.

902 **References**

- 903 Anderson, J. L., et al., 2004. The New GFDL Global Atmosphere and Land
904 Model AM2-LM2: Evaluation with Prescribed SST Simulations. *J. Climate*
905 17, 4641–4673.
- 906 Aoki, S., 2003. Seasonal and spatial variations of iceberg drift off Dronning
907 Maud Land, Antarctica, detected by satellite scatterometers. *J. Oceanogr.*
908 59, 629–635.
- 909 Bigg, G. R., Wadley, M. R., Stevens, D. P., Johnson, J. A., 1997. Modelling
910 dynamics and thermodynamics of icebergs. *Cold Reg. Sci. Technol.* 26,
911 113–135.
- 912 Boville, B. A., Gent, P. R., 1998. The NCAR Climate System Model, Version
913 One. *J. Climate* 11, 1115–1130.
- 914 Carrieres, T., Sayed, M., Savage, S., Crocker, G., 2001. Preliminary verifica-
915 tion of an operational iceberg drift model. In: POAC '01. Proc. 16th Intl.
916 Conf. Port and Ocean Engineering under Arctic Conditions. pp. 1107–
917 1116.
- 918 Cavalieri, D. J., Parkinson, C. L., 2008. Antarctic sea ice variability and
919 trends, 1979–2006. *J. Geophys. Res.* 113.
- 920 Delworth, T. L., et al., 2006. GFDL’s CM2 Global Coupled Climate Model.
921 Part I: Formulation and Simulation Characteristics. *J. Climate* 19, 643–
922 674.
- 923 El-Tahan, M. S., Venkatesh, S., El-Tahan, H., 2001. Validation and quan-
924 titative assessment of the deterioration mechanisms of Arctic icebergs. *J.*
925 *Offshore Mech. Arct. Eng.* 109, 102–108.
- 926 Gerdes, R., Hurlin, W., Griffies, S. M., 2006. Sensitivity of a global ocean
927 model to increased run-off from Greenland. *Ocean Modell.* 12, 416–435.
- 928 Gladstone, R. M., Bigg, G. R., Nicholls, K. W., 2001. Iceberg trajectory
929 modeling and meltwater injection in the Southern Ocean. *J. Geophys. Res.*
930 106 (C9), 19903–19915.

- 931 Goose, H., Fichefet, T., 1999. Importance of ice-ocean interactions for the
932 global ocean circulation: A model study. *J. Geophys. Res.* 104 (C10),
933 23337–23355.
- 934 Gordon, C., Cooper, C., Senior, C. A., Banks, H., Gregory, J. M., Johns,
935 T. C., Mitchell, J. F. B., Wood, R. A., 2000. The simulation of SST, sea
936 ice extents and ocean heat transports in a version of the Hadley Centre
937 coupled model without flux adjustments. *Clim. Dyn.* 16, 147–168.
- 938 Hack, J. J., Caron, J. M., Yeager, S. G., Oleson, K. W., Holland, M. M.,
939 Truesdale, J. E., Rasch, P. J., 2006. Simulation of the Global Hydrological
940 Cycle in the CCSM Community Atmosphere Model Version 3 (CAM3):
941 Mean Features. *J. Climate* 19, 2199–2221.
- 942 Hallberg, R., 1995. Some aspects of the circulation in ocean basins with
943 isopycnals intersecting the sloping boundaries. Ph.D. thesis, University of
944 Washington.
- 945 Hallberg, R., Gnanadesikan, A., 2006. The Role of Eddies in Determining the
946 Structure and Response of the Wind-Driven Southern Hemisphere Over-
947 turning: Results from the Modeling Eddies in the Southern Ocean (MESO)
948 Project. *J. Phys. Oceanogr.* 36, 2232–2252.
- 949 Hibler, III., W. D., 1979. A dynamic-thermodynamic sea ice model.
950 *J. Phys. Oceanogr.* 9 (4), 815–846.
- 951 Hooke, R. L., 2005. *Principles of Glacier Mechanics*. 2nd Edition, Cambridge
952 University Press.
- 953 Hunke, E. C., Dukowicz, J. K., 1997. An Elastic-Viscous-Plastic Model for
954 Sea Ice Dynamics. *J. Phys. Oceanogr.* 27, 1849–1867.
- 955 Jacka, T. H., Giles, A. B., 2007. Antarctic iceberg distribution and dissolution
956 from ship-based observations. *J. Glaciol.* 53 (182), 341–356.
- 957 Jacobs, S. S., Helmer, H. H., Doake, C. S. M., Jenkins, A., Frolich, R. M.,
958 1992. Melting of ice shelves and the mass balance of Antarctica. *J. Glaciol.*
959 38 (130), 375–387.
- 960 Jongma, J. I., Driesschaert, E., Fichefet, T., Goosse, H., Renssen, H., 2009.
961 The effect of dynamic-thermodynamic icebergs on the southern ocean cli-
962 mate in a three-dimensional model. *Ocean Modelling* 26 (1-2), 104–113.

- 963 Lancelot, C., de Montety, A., Goose, H., Becquevort, S., Schoemann, V., Pas-
 964 quer, B., Vancoppenolle, M., 2009. Spatial distribution of the iron supply
 965 to phytoplankton in the Southern Ocean: a model study. *Biogeosciences*
 966 6, 2861–2878.
- 967 Lemke, P., Ren, J., Alley, R., Allison, I., Carrasco, J., Flato, G., Fujii, Y.,
 968 Kaser, G., Mote, P., Thomas, R., Zhang, T., 2007. Observations: Changes
 969 in snow, ice and frozen ground. In: Solomon, S., Qin, D., Manning, M.,
 970 Chen, Z., Marquis, M., Averyt, K., Tignor, M., Miller, H. (Eds.), *Climate*
 971 *Change 2007: The Physical Science Basis. Contribution of Working Group*
 972 *I to the Fourth Assessment Report of the Intergovernmental Panel on Cli-*
 973 *mate Change.* Cambridge University Press, Cambridge, United Kingdom
 974 and New York, NY, USA, pp. 337–383.
- 975 Lichey, C., Hellmer, H. H., 2001. Modeling giant iceberg drift under the
 976 influence of sea ice in the Weddell Sea. *J. Glaciol.* 47, 452–460.
- 977 Løset, S., 1993. Thermal energy conservation in icebergs and tracking by
 978 temperature. *J. Geophys. Res.* 98 (C6), 10001–10012.
- 979 MacAyeal, D. R., Okal, M. H., Thom, J. E., Brunt, K. M., Kim, Y.-J., Bliss,
 980 A. K., 2008. Tabular iceberg collisions within the coastal regime. *J. Glaciol.*
 981 54 (185), 371–386.
- 982 Meehl, G., Stocker, T., Collins, W., Friedlingstein, P., Gaye, A., Gregory,
 983 J., Kitoh, A., Knutti, R., Murphy, J., Noda, A., Raper, S., Watterson, I.,
 984 Weaver, A., Zhao, Z.-C., 2007. Global climate projections. In: Solomon,
 985 S., Qin, D., Manning, M., Chen, Z., Marquis, M., Averyt, K., Tignor,
 986 M., Miller, H. (Eds.), *Climate Change 2007: The Physical Science Basis.*
 987 *Contribution of Working Group I to the Fourth Assessment Report of the*
 988 *Intergovernmental Panel on Climate Change.* Cambridge University Press,
 989 Cambridge, United Kingdom and New York, NY, USA, pp. 747–845.
- 990 Oleson, K. W., et al., May 2004. Technical description of the Community
 991 Land Model (CLM). Tech. Rep. NCAR/TN-461+STR, National Center
 992 for Atmospheric Research, Boulder, CO, 174 pp.
- 993 Opsteegh, J. D., Haarsma, R. J., Selten, F. M., Kattenberg, A., 1998. EC-
 994 BILT: a dynamic alternative to mixed boundary conditions in ocean mod-
 995 els. *Tellus Series A* 50 (3), 348–367.

- 996 Raiswell, R., Benning, L. G., Tranter, M., Tulaczyk, S., 2008. Bioavailable
997 iron in the Southern Ocean: the significance of the iceberg conveyor belt.
998 *Geochem. Trans.* 9 (7).
- 999 Reynolds, R. W., Rayner, N. A., Smith, T. M., Stokes, D. C., Wang, W.,
1000 2002. An Improved In Situ and Satellite SST Analysis for Climate. *J. Cli-*
1001 *mate* 15, 1609–1625.
- 1002 Rignot, E., Jacobs, S. S., 2002. Rapid bottom melting widespread near
1003 Antarctic ice sheet grounding lines. *Science* 296.
- 1004 Rignot, E., Kanagaratnam, P., 2006. Changes in the Velocity Structure of
1005 the Greenland Ice Sheet. *Science* 311, 986–990.
- 1006 Schodlok, M. P., Hellmer, H. H., Rohardt, G., Fahrbach, E., 2006. Weddell
1007 Sea iceberg drift: Five years of observations. *J. Geophys. Res.* 111.
- 1008 Silva, T. A. M., Bigg, G. R., Nicholls, K. W., 2006. Contribution of giant
1009 icebergs to the Southern Ocean freshwater flux. *J. Geophys. Res.* 111.
- 1010 Stammer, D., 2008. Response of the global ocean to Greenland and Antarctic
1011 ice melting. *J. Geophys. Res.* 113.
- 1012 Tsunogai, S., Watanabe, S., Sato, T. E., 1999. Is there a "continental shelf
1013 pump" for the absorption of atmospheric CO₂? *Tellus Series B* 51 (3),
1014 701–712.
- 1015 Weber, S. L., Drijfhout, S. S., Abe-Ouchi, A., Crucifix, M., Eby, M., Ganopol-
1016 ski, A., Murakami, S., Otto-Bliesner, B., Peltier, W. R., 2007. The modern
1017 and glacial overturning circulation in the Atlantic ocean in PMIP coupled
1018 model simulations. *Clim. Past.* 3, 51–64.
- 1019 Weeks, W. F., Mellor, M., 1978. Some elements of iceberg technology. In:
1020 Hussein, A. A. (Ed.), *Proceedings of the First Conference on Iceberg*
1021 *Utilization for Freshwater Production*, Iowa State University. pp. 45–98.
- 1022 Wiersma, A. P., Jongma, J. I., 2009. A role for icebergs in the 8.2 ka climate
1023 event. *Clim. Dyn.*
- 1024 Winton, M., 2000. A Reformulated Three-Layer Sea Ice Model. *J. At-*
1025 *mos. Oceanic Technol.* 17, 525–531.

- 1026 WMO, 1989. WMO Sea-Ice Nomenclature. World Meteorological Organiza-
1027 tion, Secretariat of the WMO, Geneva, Switzerland, 5th Edition.
- 1028 Worby, A. P., Geiger, C. A., Paget, M. J., Woert, M. L. V., Ackley, S. F.,
1029 DeLiberty, T. L., 2008. Thickness distribution of Antarctic sea ice. J. Geo-
1030 phys. Res. 113.

1031
1032
1033
1034
1035
1036
1037
1038
1039
1040
1041
1042
1043
1044
1045
1046
1047
1048
1049
1050
1051
1052
1053
1054
1055
1056
1057
1058
1059
1060
1061
1062
1063
1064
1065
1066
1067
1068

Table 1

Iceberg size categories with iceberg length and total thickness, mass levels, mass scaling factor and calving distribution. The mass scaling factor gives the number of icebergs represented by one Lagrangian parcel in the calculations of iceberg dynamics. The calving distribution divides the calving flux into the various iceberg size categories prescribing an iceberg size distribution at the calving site. Iceberg sizes and frequency distribution are as in Gladstone et al. (2001, their Table 2).

Figure 1

Results of experiment BERG. a) Time series of modeled calving flux (black) and iceberg melt rate (gray). The partitioning of the melt flux is depicted in red for wave erosion, blue for basal melt and green for side wall melt. b) Time series of global iceberg mass accumulated on the ocean. c) Mean annual cycle of calving (black) and iceberg melt (gray) for the southern hemisphere. d) same as panel c but for the northern hemisphere. Dashed lines mark plus/minus one standard deviation of the mean.

Figure 2

100 year average of the fresh-water flux to the ocean in mm yr^{-1} from iceberg melt in experiment BERG for icebergs originating from a) Antarctica and b) Greenland. Note the use of a logarithmic color scale. The irregular outline is a consequence of the passage of individual large icebergs.

Figure 3

Difference BERG-BITS of the fresh-water flux due to iceberg melt in mm yr^{-1} for a) the Southern Ocean and b) the North Atlantic derived from 100 year averages of the two experiments. Blue colors indicate a greater iceberg melt water flux to the ocean in BITS than in BERG, red indicates a smaller flux in BITS.

Figure 4

100 year averages of sea-ice properties and their change due to the introduction of icebergs. a) Sea-ice concentration in CTRL. b) Concentration difference of BITS-CTRL. c) In-situ sea-ice thickness in m in CTRL. d) Thickness difference in m of BITS-CTRL.

Figure 5

Difference CTRL-BITS of the salt flux from the ocean into sea ice in $10^{-6} \text{ kg m}^2\text{s}^{-1}$ for a) the Southern Ocean and b) the North Atlantic based on a 100 year mean. This salt flux is associated with frazil ice formation. Yellow-red colors (positive values) indicate less sea-ice formation in BITS due to redirecting the calving flux which ultimately lead to local sea-ice formation in CTRL, blue colors (negative values) mean more sea-ice formation in BITS where freshening and cooling now prevail due to iceberg melt farther off shore.

Figure 6

100 year averages of sea surface properties and their change due to the introduction of icebergs. a) Sea surface temperature (SST) in $^{\circ}\text{C}$ in CTRL. b) SST difference in $^{\circ}\text{C}$ of BITS-CTRL. c) Sea surface salinity (SSS) in CTRL. d) SSS difference of BITS-CTRL.

Figure 7

Annual average of the CFC-11 concentration differences BITS-CTRL in mol kg^{-1} in the Southern Ocean at 3000 m depth of model year 120, 31 years after tracer release at the surface. The CFC tracer emphasizes continental-shelf convection in the Weddell and Ross seas, which are strongly increased in the iceberg experiments (positive differences). The impact of an event of strong open ocean convection in the Weddell Sea in CTRL can also be seen (negative differences). Regions of water depths of less than 3000 m are white.

Figure 8

Ideal age tracer of ocean waters in the Atlantic Ocean at 4200 m depth in years for a) CTRL, b) BERG, and c) BITS. The annual average of model year 120 is shown.

Figure 9

Comparison of simulated (blue, from experiment BERG) and observed calving rates (red). a) 29 calving locations around Antarctica given by Gladstone et al. (2001). b) Glacial discharge published by Rignot and Kanagaratnam (2006) concentrated in 9 main regions.

Figure 10

Partitioning of the fresh-water flux entering the Southern Ocean: a) fraction of iceberg melt, b) fraction of sea-ice melt, and c) fraction of precipitation

1107 including liquid runoff. Results of the BITS experiment are shown. In panels
1108 a and b white areas indicate values falling below 0.005, in panel c this marks
1109 values greater than 0.995.